Available online at www.sciencedirect.com

ScienceDirect

journal homepage: www.elsevier.com/locate/he

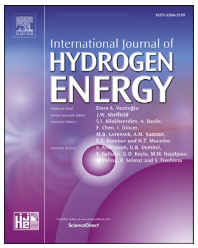

Artificial neural network based chemical mechanisms for computationally efficient modeling of hydrogen/carbon monoxide/kerosene combustion

Jian An [a,b], *Guoqiang He* [a], *Kaihong Luo* [b], *Fei Qin* [a,*], *Bing Liu* [a]

[a] *Science and Technology on Combustion, Internal Flow and Thermal-structure Laboratory, Northwestern Polytechnical University, Xi'an, Shaanxi, 710072, PR China*

[b] *Department of Mechanical Engineering, University College London, London, WC1E 7JE, United Kingdom*

HIGHLIGHTS

- An ANN-based solver was developed to take over the chemistry calculation.
- The ANN-based solver shows excellent consistency with the conventional CFD results.
- 8~20 times speedup is achieved by using ANN-based solver.
- Computational cost of the ANN-based model increases linearly.

ARTICLE INFO

Article history:
Received 5 May 2020
Received in revised form
9 July 2020
Accepted 10 August 2020
Available online 1 September 2020

Keywords:
Hydrogen combustion
Kerosene combustion
Supersonic combustion
Artificial neural network (ANN)
Rocket-based combined cycle (RBCC)

ABSTRACT

To effectively simulate the combustion of hydrogen/hydrocarbon-fueled supersonic engines, such as scramjet and rocket-based combined cycle (RBCC) engines, a detailed mechanism for chemistry is usually required but computationally prohibitive. In order to accelerate chemistry calculation, an artificial neural network (ANN) based methodology was introduced in this study. This methodology consists of two different layers: self-organizing map (SOM) and back-propagation neural network (BPNN). The SOM is for clustering the dataset into subsets to reduce the nonlinearity, while the BPNN is for regression for each subset. Compared with previous studies, the chemical reaction mechanism involved in this study is more complex, therefore, the particle swarm optimization (PSO) method is employed for accelerating training process in this study. Then we were committed to constructing an ANN-based mechanism of hydrogen and kerosene for supersonic turbulent combustion and verifying it in a practical RBCC combustion chamber. The training data was generated by RANS simulations of the RBCC combustion chamber, and then fed into the SOM-BPNN with six different topologies (three different SOM topologies and two different BPNN topologies). Through LES simulation of the Rocket-Based Combined Cycle (RBCC) combustor, the six ANN-based mechanisms were verified. By comparing the predicted results of six cases with those of the conventional ODE solver, it is found that if the topology is properly designed, high-precision results in terms of ignition, quenching and mass fraction prediction can be achieved. As for efficiency, 8~20 times speedup of the chemical system integration was achieved, which will greatly improve the computational efficiency of combustion simulation of hydrogen/carbon monoxide/kerosene mixture.

* *Corresponding author.*
E-mail address: qinfei@nwpu.edu.cn (F. Qin).

https://doi.org/10.1016/j.ijhydene.2020.08.081

Introduction

Rocket-based combined cycle (RBCC) engines seamlessly combine the advantages of high thrust/weight ratio of rocket engines and high specific impulse of jet engines to effectively operate at multiple modes ranging from take-off, high altitude hypersonic cruise, to orbit [1]. The RBCC engines operate in multi working modes, which consists of the rocket–ejector mode, ramjet mode, scramjet mode and pure-rocket mode. Its highly integrated design and superior performance makes it most likely to be used in the next generation of Hypersonic RLV, and one of the most promising propulsion systems for Single Stage To Orbit (SSTO) [2]. With the deepening of research on combustion process and the increasing demand for efficient design, high-fidelity numerical simulation has attracted more and more attention [3,4]. In RBCC engines, the mode transition is mainly adjusted by the primary rocket. The key to numerical simulation, therefore, is to capture the complex mixing and combustion process between the exhaust of the rocket (mainly containing hydrogen and carbon monoxide) and the incoming air and the injected kerosene. However, to effectively simulate the combustion of these processes, a detailed mechanism for chemistry is usually required [5]. The mechanism mathematically represents a large set of nonlinear stiff ordinary differential equations (ODEs) and must be integrated over every spatial point and every time step, hence, the computational cost of such ODEs in unsteady, three-dimensional reacting flows is prohibitive, even as a high-performance computing system have become accessible within the last decade. There are several ways to accelerate the calculation. Using reduced mechanisms is a widely used method to overcome this limitation [6]. Examples are the methodologies for generating pre-reduced skeleton mechanisms, such as the multi-generation path flux analysis (PFA) method [7], the direct relation graph (DRG) method [8], or the DRG with error propagation (DRGEP) method [9], and approaches for generating local mechanisms for each grid and time step based on local thermodynamic conditions, namely the dynamic adaptive chemistry (DAC) method [10,11].

Under the assumption that the flow field and chemistry are loosely coupled, the thermochemical states can be precomputed or stored for reuse in real time, thus reducing the expensive real time calculations in the simulation process. A straightforward approach is the lookup table (LUT) method proposed by Chen et al. [12], which directly stores thermodynamic states and reuses them. A pivotal approach for tabulation is the in situ adaptive tabulation (ISAT) [13], where the table of thermochemical states is generated on-the-fly and reused in later time steps using a binary tree algorithm. Although many efforts, such as the most recently used (MRU) and dynamic pruning strategy (DP) [14], have been made to improve the efficiency of the modification and retrieve of the table, the performance of ISAT would decrease significantly when dealing with large-scale unsteady numerical simulations like LES due to the extremely big table required [11].

Following this avenue, a good choice to overcome the shortcomings of chemistry tabulation is to use artificial neural networks (ANNs) to store thermochemical states. ANNs can efficiently represent the non-linear relationship between the input and output data and has been applied to the control [15–18], optimization [18,19], modeling [20–22] and prediction [23–27] of combustion system. For modeling the change of thermodynamic space, Christo et al. [28] took the early attempts to apply ANNs to represent chemical reactions, using a three-step chemistry mechanism for hydrogen turbulent combustion. The runtime and memory storage requirements were significantly reduced compared to the traditional look-up table technique as well as the direct integration approaches. Subsequently, a reduced mechanism contained 4 steps and 8 species (CH4, O2, CO2, H2O, CO, H2, H and N2) was employed as the target of ANN. By comparing the results of direct integration with those of a large number of random samples, a good agreement is obtained [29]. Blasco et al. [30] applied the ANNs for a reduced, 5 steps and 8 species mechanism for methane–air combustion, which is derived from the GRI 2.11 mechanism. In this work, they proposed to divide the samples of thermodynamics space into sub-domains and use multiple ANNs with the aim to get a dedicated ANN for each sub domain, resulting in a two-layer topology network. In the first layer, self-organizing map (SOM), a technique that can divide high dimensional data into several patterns by calculating the Euclidean distance, was applied to the automatic partitioning. Combined with the ANNs for representation, the SOM-ANN topology was established and tested by simulating a Partial Stirred Reactor (PaSR). The presented approach was validated and encouraging results were reported.

Furthermore, Chatzopoulos and Rigopoulos [31] and Franke et al. [32] developed a method of combining the Rate-Controlled Constrained Equilibrium (RCCE) with the SOM-ANN for a mechanism of CH4–air combustion with 16 species. The training datasets were generated from an abstract problem based on the laminar flamelet equation and consist of the thermodynamics states with different mixture fractions and strain rates. After training, the simulation results show that RCCE-SOM-ANN topology can reduce the CPU time by about two orders of magnitude with excellent accuracy. In the above work, the target mechanism for ANN is relatively small (up to 16 species to our knowledge) and is for simple fuels like hydrogen or methane. However, most of the fuels used in engineering applications are complex hydrocarbon fuels, and their mechanisms usually involve hundreds to thousands of species. In addition, most of the trained ANN models are

verified using model flames, such as Sandia Flames or Sydney Flames. In the case of supersonic mixing and combustion of hydrogen/carbon monoxide/kerosene, its performance has yet to be tested. The simulation of supersonic combustion is highly demanding because a small error of the reaction can cause large disturbances. Therefore, it will be very challenging to establish an ANN-based chemical mechanism suitable for supersonic combustion.

In this study, we are committed to constructing an ANN-based mechanism for supersonic turbulent combustion and verifying it in a practical RBCC combustion chamber. The remainder of this paper is organized as follows. Section Methodology introduces the methodology involved in this study. Section Application of SOM-BPNN method in an RBCC combustor briefly describes test cases and the numerical approach. Section Results and discussion presents performance analyses. Section Conclusions concludes this paper.

Methodology

Overview

To simulate a reactive flow, the spatially discretized governing equations with the Strang-based splitting scheme [33] can be expressed as:

$$\frac{d\mathbf{\Phi}}{dt} = \mathbf{M}(\mathbf{\Phi}) + \mathbf{S}(\mathbf{\Phi}) \tag{1}$$

where $\mathbf{\Phi}$ is the vector of the thermo-chemical composition, including, e.g., temperature and species concentrations, and $\mathbf{M}$ and $\mathbf{S}$ represent the transport and chemistry terms, respectively. With a Strang-based splitting scheme [33], integration of chemical reactions is separated from that of other physical processes. The transport terms which include unsteady, convection and diffusion terms are described by a second order PDE system of an unreactive flow, while the chemical reaction source terms are described by a first-order ordinary differential equation (ODE) system, which can be expressed as:

$$\frac{d\phi}{dt} = S(\phi) \tag{2}$$

where ϕ is the vector of the thermo-chemical composition, i.e. pressure p, temperature T, and the vector $\mathbf{Y}$ of species mass fractions; and S is its rate of change due to chemical reactions. To determine the thermochemical composition altered by chemical reactions over a time step, the CFD solver loops over all the computational cells and then calculates the integration of each reaction step, typically using stiff ODE solvers. To determine the thermochemical composition of a chemical reaction that changes over a time step, the integrator need to loop over all the computational cells. However, the thermochemical states in many cells are similar, and these repeated calculations consume a lot of computational resources. Therefore, to speed up the integration, an effective way is to store and reuse the map of the change of thermochemical states.

A two-layer structure as shown in Fig. 1, SOM-BPNN, was deployed in this work, in which SOM was responsible for classifying datasets because otherwise it would be difficult to obtain satisfactory model by using only one ANN. Furthermore, the back-propagation artificial neural network (BPNN), one type of ANN, was used to regress each subclass.

Sample generation

The sample generation is the first step. By learning the samples, the neural network can approximate the complex nonlinear system, that is, the applicability of the obtained model depends on the training samples. For any chemical reaction, the thermodynamic state at time t, $\phi(t)$, and that after a time step, $\phi(t+\Delta t)$, are a pair of samples. When a large number of samples through a pre-calculation were collected to form a dataset, it can represent the entire process of chemical integration. In this study, the dataset was generated by a pre-simulated case as detailed in Section Application of SOM-BPNN method in an RBCC combustor.

The SOM concept and implementation

Represented by the dataset, the change of the thermochemical state driven by the chemical reaction is a high-dimensional system with complex nonlinear behavior. Although it is theoretically possible to employ only a single ANN to deal with such a problem, it is not a good choice because of poor computational efficiency and accuracy. Therefore, the SOM technique was introduced to divide the data set into several clusters [34]. The SOM is based on unsupervised learning, typically employed to perform pattern classification tasks. For the training process, once the samples are fed into the SOM, the algorithm adjusts the position of each neuron to minimize the Euclidean distance from more input samples. After the training phase, each neuron is the center of some input, representing a part of the input space. Meanwhile, the sum of distance of all samples to their center can be quantified by Eq. (2), the quantization error, where x_i and m_{i-best} represent the i-th sample and its best match neuron. The smaller the Q error, the more refined the classification. Finally, by finding the neuron with the smallest Euclidean distance from the input sample, the trained self-organizing tree model can assign the new sample to the subdomain.

$$Q = \sum_i \|x_i - m_{i-best}\|^2 \tag{3}$$

The BPNN concept and training

Through the previous step, the sample set was divided into subsets, and each subset has a BPNN for regression. BPNN is a kind of ANN widely used in regression analysis, which can deal with non-linear relations efficiently [35]. It usually has three parts: one input layer, one or more hidden layers and one output layer; and each of these layers has several neurons. These layers are connected by weights and biases

matrices. A BPNN can provide a regression between the inputs and outputs as:

$$\mathbf{X} \rightarrow \mathbf{Y} \tag{4}$$

where the output of one neuron is calculated by the following equation:

$$o_i = \varphi(net_i) = \varphi\left(\sum_{j=1}^{N} w_{ij} x_j + \theta_i\right) \tag{5}$$

where o_i and θ_i represent the response and the bias of the i-th neuron, respectively. $w = (w_{ij})_{N\times L}$ is the matrix of the connection weights. $\varphi(\bullet)$ represents the activation function of BPNN. The output of a neuron is the input to a neuron in the next layer. In this study, the tanh was used as the activation function defined as:

$$\varphi(x) = tanh(x) \tag{6}$$

According to Eq. (5), the weights play an important role in the calculation process. The fitting precision depends on the weight values. However, the weights and biases are randomly initialized at the beginning. If the initial values are not suitable, the training may not converge. Therefore, the particle swarm optimization (PSO) method is employed in choosing a better initial value in this study because the BPNN-PSO has excellent performance in the accelerating convergence [35]. The PSO is a population-based optimization method that simulates the social behavior of birds. The PSO method is randomly initialized with a swarm of particles which are potential solutions and then searches the optima and update generations. Each particle has two main parameters: velocity and position. Here, velocity and position are representative of the shift distance (including orientation) and current values. During the iteration, the velocity and position of each particle are updated according to the following formula:

$$v_i^{n+1} = \omega v_i^n + c_1 r_1^n \left[p_{i,p_b best}^n - p_i^n\right] + c_2 r_2^n \left[p_{gbest}^n - p_i^n\right] \tag{7}$$

$$p_i^{n+1} = p_i^n + v_i^{n+1} \tag{8}$$

where v_i^n and v_i^{n+1} are velocities of particle i at iterations n and $n+1$; p_i^n and p_i^{n+1} are positions of particle i at iterations n and $n+1$; ω is the inertia weight. When we use the PSO algorithm as a BPNN training optimization method, the fitness value of the particles can be defined as the root mean square of errors (RMSE):

$$RMSE = \sqrt{\frac{1}{N}\sum_{i=1}^{N}\left(y_i^{exp} - y_i^{pre}\right)^2} \tag{9}$$

where N represents the total number of training data points, y_i^{pre} is the i-th output of network, y_i^{exp} are the actual values. After a couple of iterations, the final particle's position vector represents the weights and biases of the neuron when the fitness reaches the preset value. A complete algorithm can be found in Refs. [36,37]. After initialization, the Adam optimizer [38], which is an efficient algorithm, is used to train each BPNN. When this is done, a complete SOM-BPNN-based mechanism is established and ready to use.

Application of SOM-BPNN method in an RBCC combustor

In this section, the SOM-BPNN was applied to represent a skeletal mechanism with 41 species and 132 elemental reactions [39]. This skeletal mechanism is derived from a detailed kerosene high temperature mechanism of $C_{10}H_{22}$ consisting of 121 species and 866 reactions [40] and has been verified to have good accuracy for hydrogen/carbon monoxide/kerosene combustion mixtures [39]. As shown in Fig. 2,

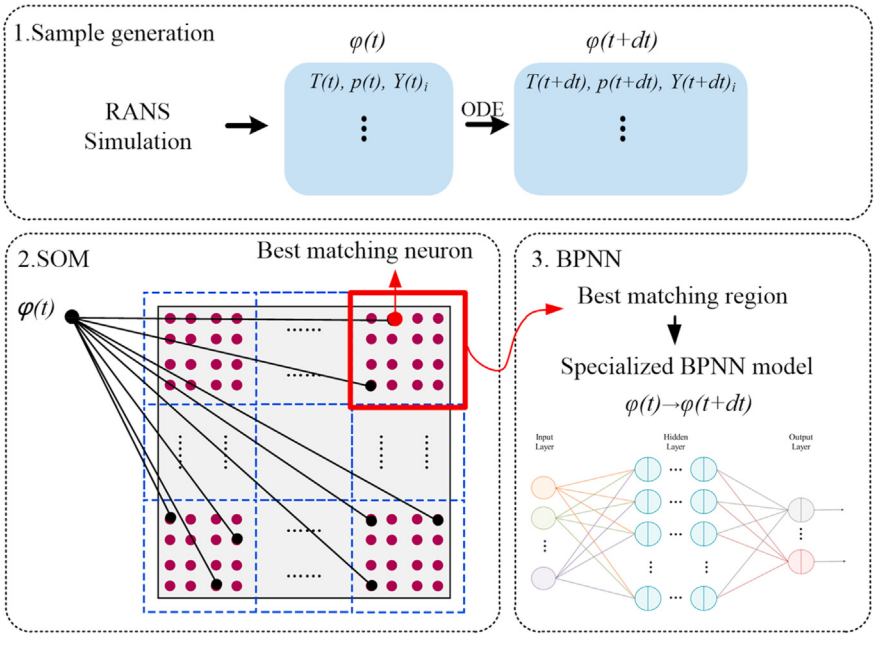

Fig. 1 – Schematic of the training process of the SOM- BPNN topology.

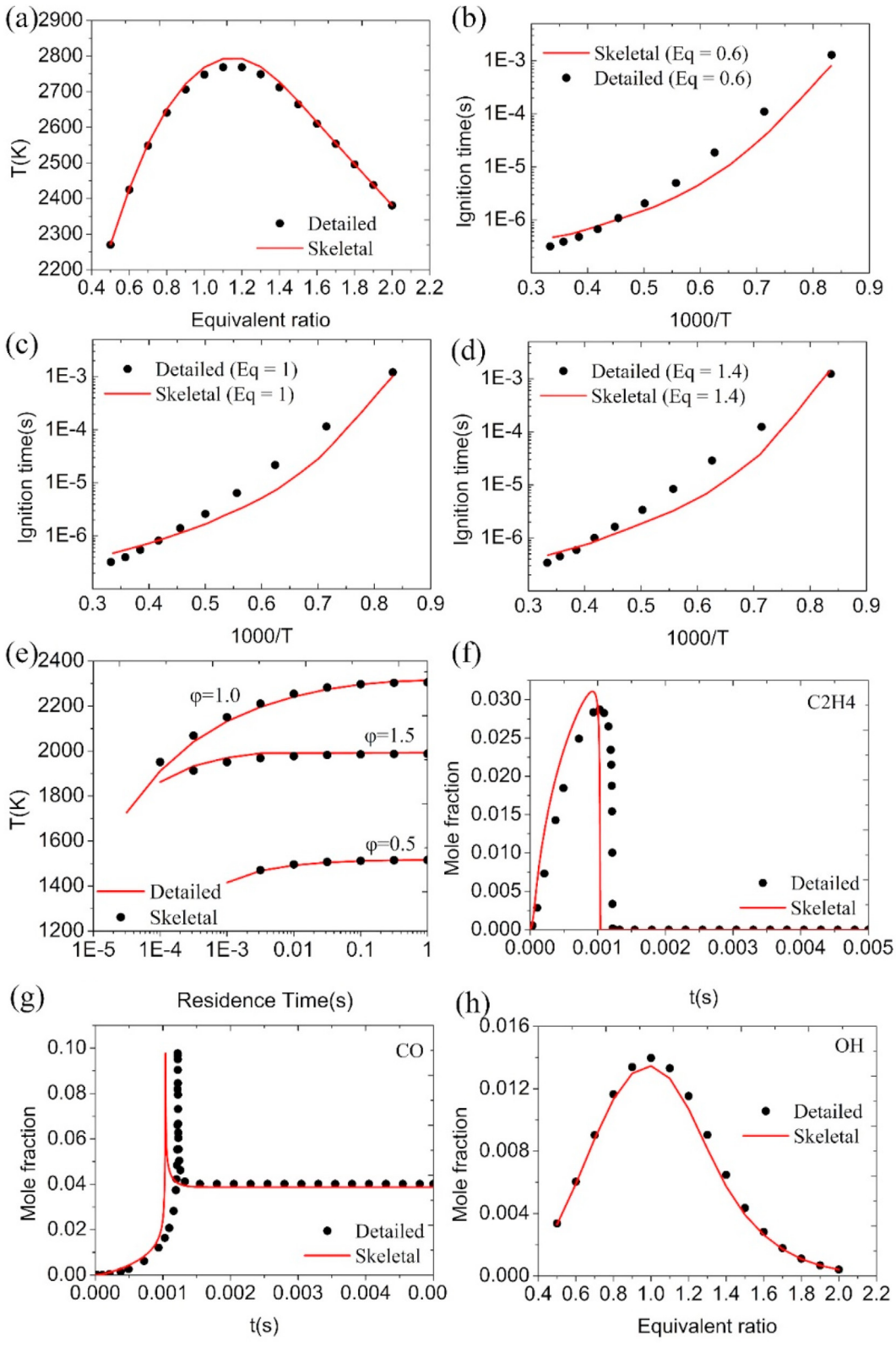

Fig. 2 – Comparisons between the skeletal mechanism and the detailed mechanism.

The comparisons of flame temperature, ignition delay time, ignition process and extinction predicted by the skeletal mechanism show an overall good accordance with the detailed mechanism [39].

As described in Section Sample generation, the pre-calculated case for sample generation is a RANS simulation of a full-scale RBCC engine corresponding to the flight condition at $Ma = 5.5$ [39]. As shown in Fig. 3, it has a main strut, an

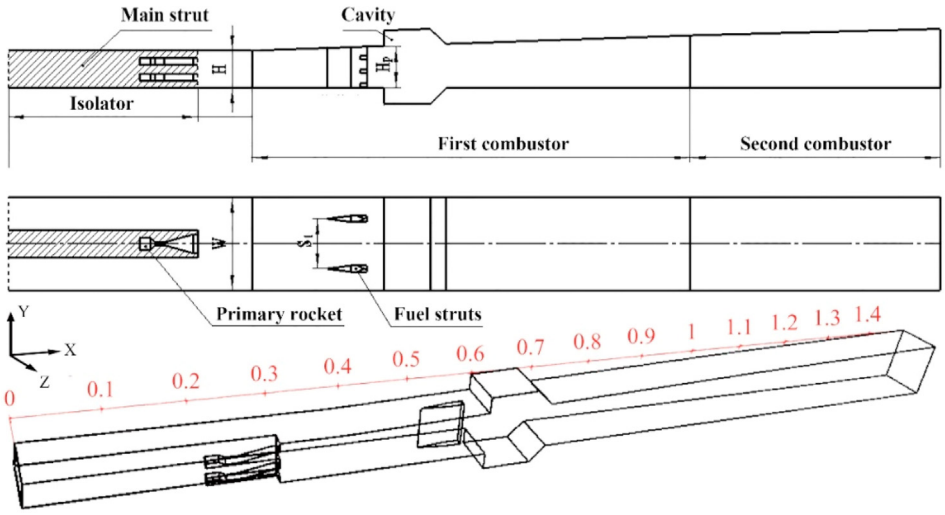

Fig. 3 – Configuration of the RBCC combustor.

isolator, a primary rocket, two struts for secondary fuel injection and flame stabilization, two cavity flame holders and multi-stage rectangular combustors. The main strut provides the Mach number required for the inlet of the isolator, which is used to reduce the interaction between the inlet and the combustion chamber. The primary rocket is a fuel-rich gas generator (94% CO and 6% H2) that acts as an igniter and flame holder for secondary fuel combustion. At the same time, the combustion chamber is designed to have an expanded shape to widen the operating range. This configuration contains complex physicochemical phenomena such as spray, supersonic turbulent combustion, etc. The inlet boundary conditions are enumerated in Table 1. The sprayFoam solver in OpenFOAM 16 is used to conduct simulation with the k-Omega SST turbulence model and PaSR combustion model [41]. It is based on the conjecture that any turbulent flow can be divided into fine structures (*) and surroundings (0), interacting through the balance equations. Most of dissipation and mixing as well as chemical reactions take place in the fine structures, where reactants are mixed at scales of molecular level. Therefore, each cell can be viewed as a partially stirred reactor containing the fine structures, which is ideally regarded as a Perfectly Stirred Reactor (PSR), exchanging mass and energy with the surroundings. This combustion model or its derivation has been proved to be effective for the modeling of supersonic turbulent combustion and can accurately capture such phenomena as local ignition and extinction [5,41,42].

The chemical alterations, including the species mass fractions, temperature, and pressure (for a total of 43 dimensions in this case), were recorded throughout the simulation to generate the entire data set, which is then used as input to the SOM-BPNN. The simulation was conducted for 1 ms with time step of 2×10^{-8} s, which was enough time to obtain sufficient samples. Finally, the obtained dataset was divided into a training set (60% of the samples) and a test set (40% of the samples). As for the performance of SOM, three different topologies were tested with 30×30 neurons, 40×40 neurons and 50×50 neurons, respectively. Using the trained SOM, the dataset was divided into subsets, and then each subset was assigned a BPNN for representation. Two alternative topologies are carried out and listed in Table 2. The notation, e.g. "43–43", means there are 2 hidden layers and 43 neurons are included in each layer. Combined with the SOM scheme, 6 cases were finally implemented.

It is worth noting that choosing the parameters of SOM (the neuron number) and BPNN (the number of hidden layers and neurons per layer) is a trade-off. Because an overly complex topology can lead to overfitting and more computational costs, while oversimplified one can result in low performance. However, there is not much literature and research on parameter setting for reference. Franke et al. [32] tested the effectiveness of a 400/100/25-neuron SOM paired with a 2-layer 30-neuron ANN to model a 16-species methane mechanism. The results show that using 100-neuron SOM is sufficient for their case. Considering that the number of species in this study increased to 41 and faced more complex turbulent supersonic flows, we increased the topological scale of SOM and BPNN. After trying different numbers of SOM and BPNN neurons, the current parameters are finally determined. The Q error and the mean testing error, which are the parameters to

Table 1 – Simulation conditions.

Inlet		Rocket Inlet		Second-fuel
Temperature, K	Mass, g/s	Temperature, K	Mass, g/s	Mass, g/s
1300	4000	1900	120 (94% CO, 6% H2)	200 (100% Kerosene)

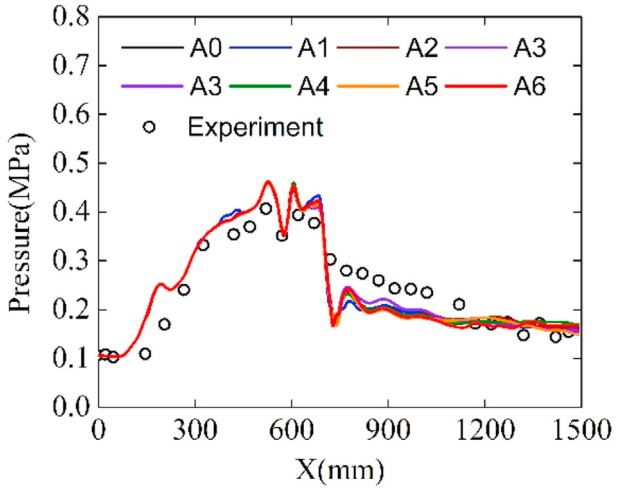

Fig. 4 – Side surface pressures of simulation (cases A0-A5) and experiment [39].

measure the training accuracy of SOM and BPNN, respectively, are also given in Table 2. The mean testing error was calculated by Eq. (10) by using test set,

$$RMSE = \sqrt{\frac{1}{N}\sum_{i=1}^{N}\left(y_i^{exp} - y_i^{pre}\right)^2} \tag{10}$$

where N represents the total number of training data points, y_i^{pre} is the i-th predicted value of the SOM-BPNN network, y_i^{exp} are the actual value. The results show that the maps using 625 and 400 subdomains exhibited lower error than the one with 225 SOM subdomains. Meanwhile, for a same SOM topology, the error of the 3-layer BPNN is also lower than that of the 2-layer, e.g. A3 vs. A4. Finally, the difference between A5 and A6

Table 2 – Configuration of SOM-BPNN and test cases.

Case No.	SOM neurons/ subdomain	Q error	BPNN topology	Testing error
A0	ODE	–	–	–
A1	30 × 30/225	0.07406	43–43	7.1×10^{-04}
A2			43–43–43	2.6×10^{-04}
A3	40 × 40/400	0.06068	43–43	6.7×10^{-05}
A4			43–43–43	3.7×10^{-05}
A5	50 × 50/625	0.05265	43–43	2.4×10^{-05}
A6			43–43–43	2.3×10^{-05}

is very small, indicating that there was no need for further refinement of the topology of SOM and BPNN.

Results and discussion

In this part, the models developed above were applied to the RBCC mentioned in the previous section and the results are then discussed. Unlike the training samples, LES with 12 million structured cells is performed. First, as shown in Fig. 4, the wall pressure distributions of all cases are validated using experimental data, which was collected in a direct connect supersonic combustion test platform assembled in Science and Technology on Combustion, Internal Flow and Thermal-structure Laboratory (Northwestern Polytechnical University, Xi'an, China) [39,43]. The trend of the pressure distributions is consistent with the experimental results, indicating that the model used can simulate real working conditions and that different ANN topologies have slightly influenced on pressure prediction.

Furthermore, Fig. 5 shows a comparison of instantaneous temperature and mass fraction distributions of selected

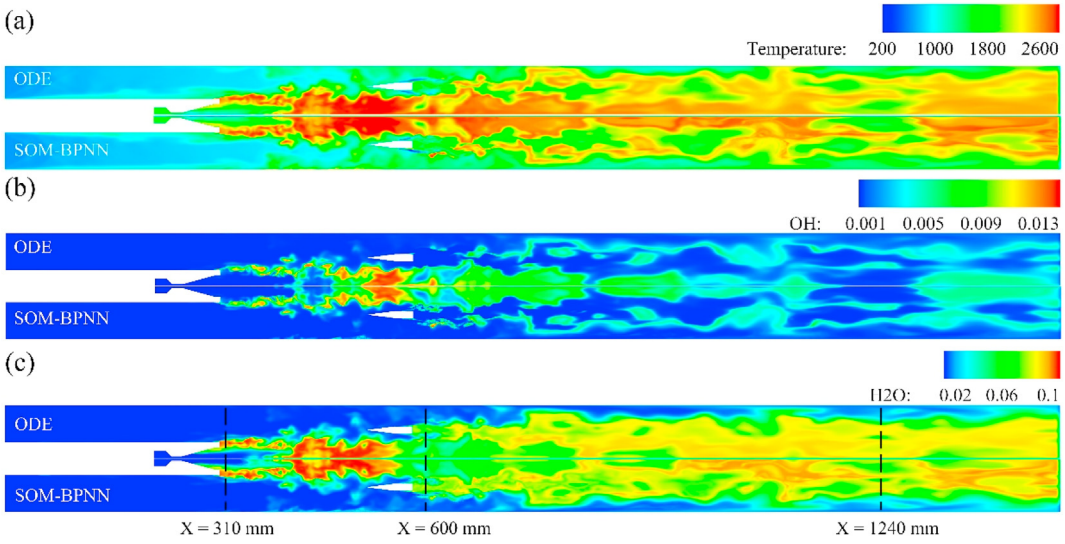

Fig. 5 – Instantaneous temperature and mass fraction distributions of OH and H_2O of Case A0 (top) and Case A1 (bottom).

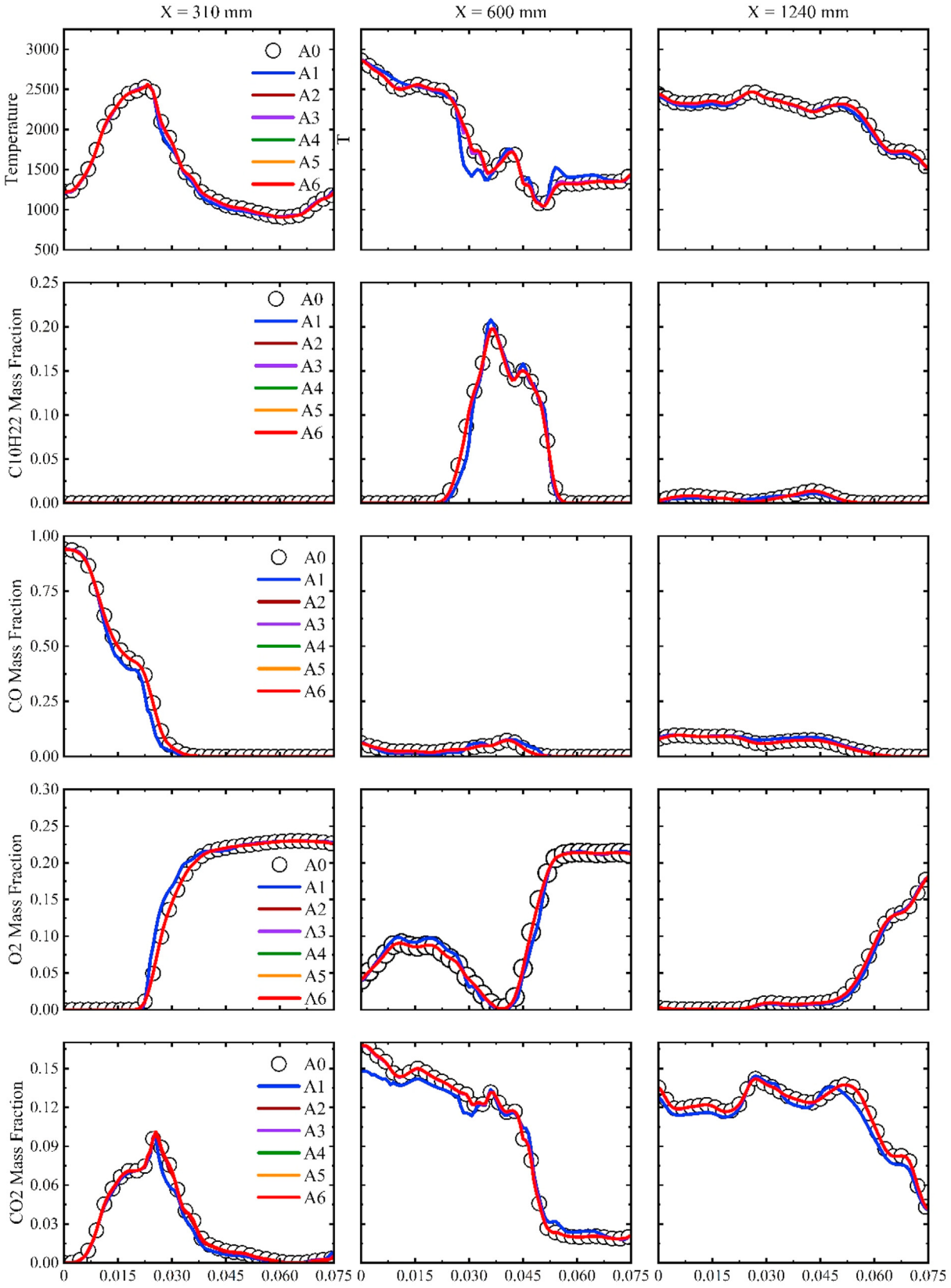

Fig. 6 – Time-averaged temperature and mass fraction profiles of selected species at X = 310 mm, X = 600 mm and X = 1240 mm.

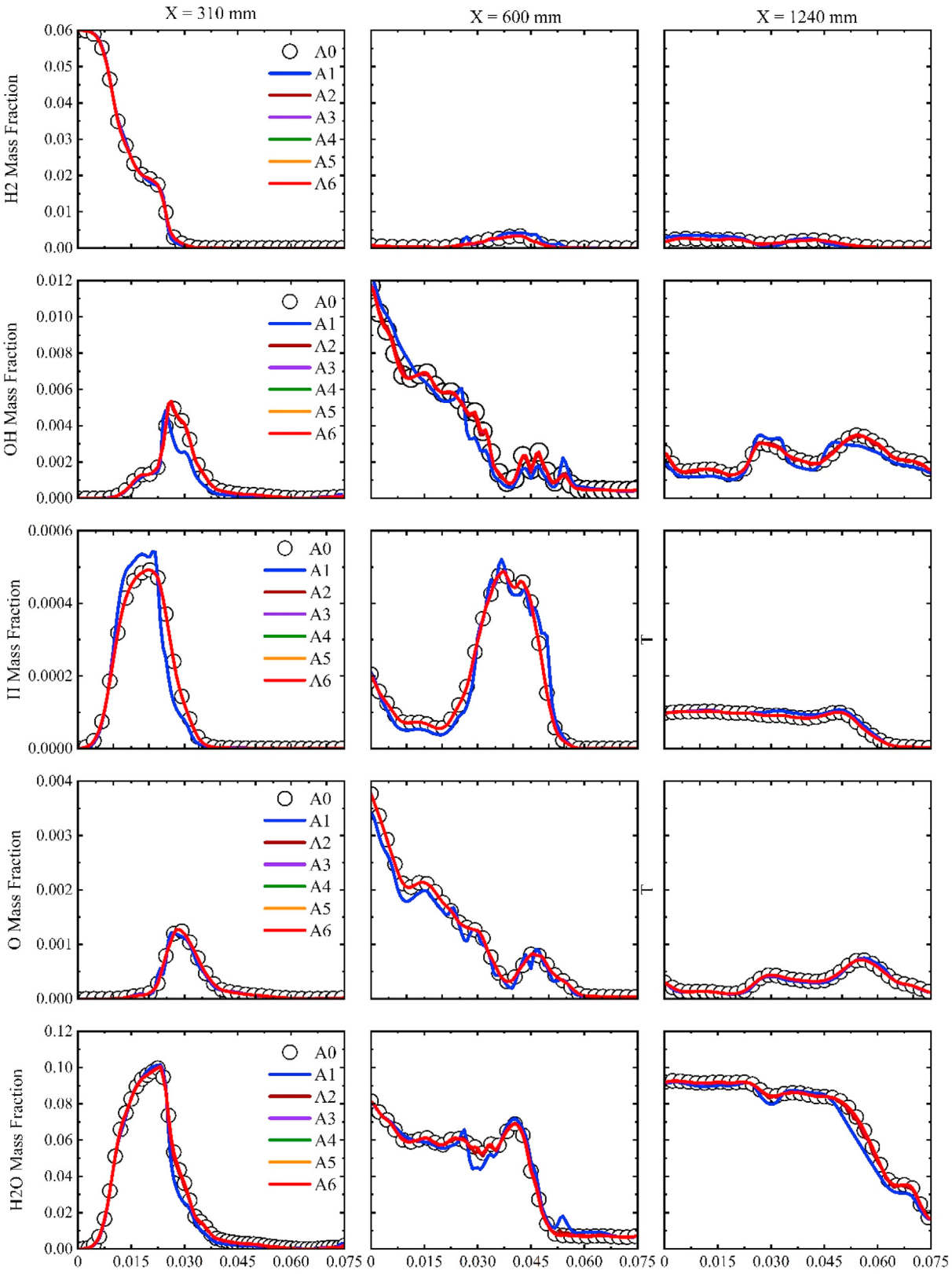

Fig. 7 – Time-averaged mass fraction profiles of selected species at X = 310 mm, X = 600 mm and X = 1240 mm.

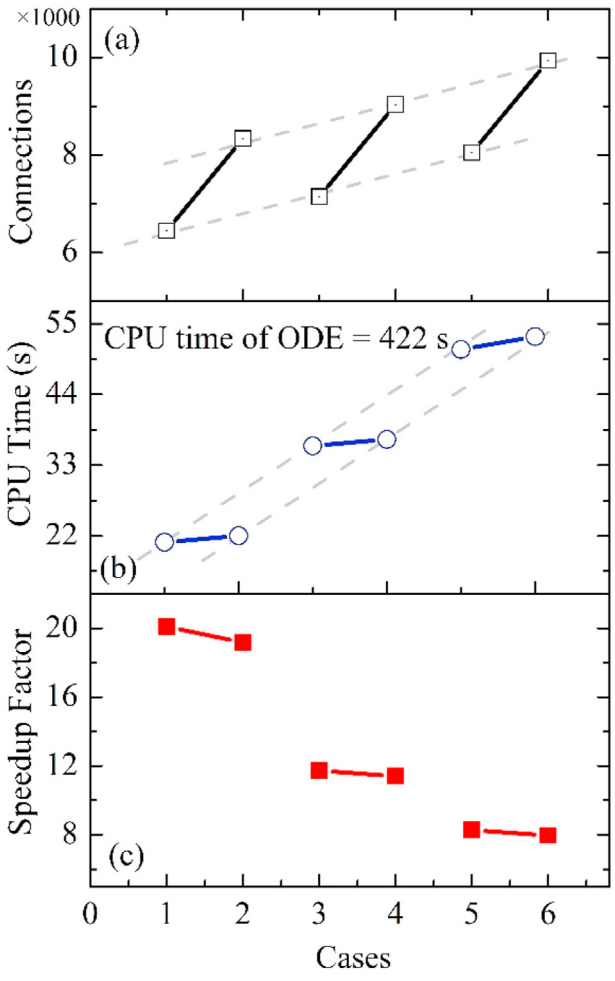

Fig. 8 – (a) Number of connections, (b) CPU time and (c) Speedup factor of different cases.

species in cases A0 and A2. Simulations using the original chemistry and the ANN-based chemistry both capture the same flame structures as well as primary combustion (guided by primary rocket) and secondary combustion (triggered by the secondary fuel).

To assess the accuracy of different topologies in more detail, time-averaged temperature and mass fraction profiles of selected species at three locations were further extracted (X = 310 mm, X = 600 mm and X = 1240 mm, marked in Fig. 5). These three locations represent different stages: 1) Combustion guided by the high temperature and fuel-rich gas flow exhausted from the primary rocket; 2) Mixing and intense combustion of secondary fuel injected by struts; 3) End of the combustion process. As shown in Figs. 6 and 7, in the first state, the curves show a sharp change, because the gas from the primary rocket is rich in reactive species (OH, CH_2O, etc.), which will start an intense reaction in an instant. Then, as the kerosene is injected and cracked, more reactants are added and burned, giving the double-peak curves (X = 600 mm). One of the peaks is derived from the upstream reaction product, while the other comes from the injected kerosene. Eventually, as shown in the figures of X = 1240 mm, oxygen cannot be mixed with the center stream in time due to the supersonic speed, so that some of the reactants are not consumed.

In terms of the accuracy of the six ANN-based mechanisms, five of them have good consistency with conventional ODE result (Case A0), while the case with the fewest neurons (Case A1) does not. As for Case A1, its temperature distribution and mass fraction distribution of selected species is inconsistent with Case A0. Given that Case A1 is the simplest topology in all SOM-BPNN cases, it shows that the learning ability of this topology is not enough to support the complexity of this mechanism for supersonic combustion, which leads to this unsatisfactory result. However, the remaining five ANN-based mechanisms can successfully represent the mass distribution of intermediate species and characterize local ignition and quenching caused by turbulent fluctuations.

The simulation of these phenomena is highly demanding because, for supersonic combustion, a small error can cause large disturbances. For example, the ignition delay time calculated by the mechanism will determine whether or not a stable and self-sustaining combustion can be formed in the supersonic flow. Furthermore, the predicted values of OH, CO, H, O and H2O, which are important intermediates and products of hydrogen/carbon monoxide/kerosene combustion, are highly consistent with the original model. This proved that the five ANN-based mechanisms could handle the combustion process of hydrogen/carbon monoxide/kerosene.

The above results verified the accuracy of the new model, while its other performance metrics need to be demonstrated. Fig. 8(a) shows the number of connections of different SOM-BPNN topologies. It represents the operations that the neural network needs to perform in calculating the chemical reactions. The results demonstrate that there is a linear relationship between the number of connections and the number of layers or the number of SOM neurons. Furthermore, combined with Fig. 8(b), the computational cost is also linearly related to the complexity of SOM-BPNN, while the calculation using ODE for reaction is proportional to the square of the species number. Finally, compared with directly solving 41 mechanisms, 8 to 20 times speedup is achieved by using different ANN topologies as shown in Fig. 8(c). Meanwhile, these results indicate that there is an optimal topology that can balance efficiency and accuracy, which is Case A2 in our study. These results encourage the application of this approach to more complex mechanisms.

Conclusions

In this study, for the first time, we constructed an ANN-based chemical mechanism of hydrogen/carbon monoxide/kerosene mixture with 41 species through a SOM-BPNN topology and verified it in a practical RBCC combustion chamber. Compared with previous studies, the chemical reaction mechanism involved in this study is more complex, therefore, the particle swarm optimization (PSO) method is employed for accelerating training process in this study. Six topologies with

different numbers of SOM neurons and BPNN layers were carried out to represent the dataset, which were generated by RANS simulations of the RBCC combustion chamber with less computational intensity. After training, the new modeling framework was applied to the LES simulation of the RBCC combustion chamber.

In terms of accuracy, five ANN-based models provide excellent consistency with the conventional ODE solver, while the case with the fewest neurons (Case A1) does not. As for efficiency, the CPU time of the ANN-based model was reduced typically by 8~20 times, compared with the conventional ODE solver with the 41 species skeleton mechanism. These results indicate that there is an optimal topology that can balance efficiency and accuracy, which is Case A2 in our study. It can achieve a speedup of 19 times while having a good calculation accuracy. Moreover, the computational cost of the ANN-based model is linearly proportional to the number of connections, while that of the ODE solver for reaction increases with the square of the species number, indicating a great potential of ANN-based models for more complex fuels.

Declaration of competing interest

The authors declare that they have no known competing financial interests or personal relationships that could have appeared to influence the work reported in this paper.

Acknowledgments

Support from the UK Engineering and Physical Sciences Research Council (Grant Nos. EP/R029598/1 and EP/S012559/1) and the China Scholarship Council (CSC) (File No. 201806290091) is gratefully acknowledged.

Appendix A. Supplementary data

Supplementary data to this article can be found online at https://doi.org/10.1016/j.ijhydene.2020.08.081.

REFERENCES

[1] Cecere D, Giacomazzi E, Ingenito A. A review on hydrogen industrial aerospace applications. Int J Hydrogen Energy 2014;39:10731–47.
[2] Yang Q, Shi W, Chang J, Bao W. Maximum thrust for the rocket-ejector mode of the hydrogen fueled rocket-based combined cycle engine. Int J Hydrogen Energy 2015;40:3771–6.
[3] Jin T, Luo K, Lu S, Fan J. DNS investigation on flame structure and scalar dissipation of a supersonic lifted hydrogen jet flame in heated coflow. Int J Hydrogen Energy 2013;38:9886–96.
[4] Liu C, Wang Z, Sun M, Wang H, Li P, Yu J. Characteristics of the hydrogen jet combustion through multiport injector arrays in a scramjet combustor. Int J Hydrogen Energy 2018;43:23511–22.
[5] Liu B, He G-Q, Qin F, An J, Wang S, Shi L. Investigation of influence of detailed chemical kinetics mechanisms for hydrogen on supersonic combustion using large eddy simulation. Int J Hydrogen Energy 2019;44:5007–19.
[6] Liu B, He G-q, Qin F. Simulation of supersonic Ethylene–Hydrogen and air auto-ignition flame using skeletal mechanism. Acta Astronaut 2018;152:521–33.
[7] Sun WT, Chen Z, Gou XL, Ju YG. A path flux analysis method for the reduction of detailed chemical kinetic mechanisms. Combust Flame 2010;157:1298–307.
[8] Lu TF, Law CK. A directed relation graph method for mechanism reduction. Proc Combust Inst 2005;30:1333–41.
[9] Pepiot-Desjardins P, Pitsch H. An automatic chemical lumping method for the reduction of large chemical kinetic mechanisms. Combust Theor Model 2008;12:1089–108.
[10] Liang L, Stevens JG, Farrell JT. A dynamic adaptive chemistry scheme for reactive flow computations. Proc Combust Inst 2009;32:527–34.
[11] An J, He G, Qin F, Wei X, Liu B. Dynamic adaptive chemistry with mechanisms tabulation and in situ adaptive tabulation (ISAT) for computationally efficient modeling of turbulent combustion. Combust Flame 2019;206:467–75.
[12] Chen JY, Kollmann W, Dibble RW. Pdf modeling of turbulent nonpremixed methane jet flames. Combust Sci Technol 1989;64:315–46.
[13] Pope SB. Computationally efficient implementation of combustion chemistry using in situ adaptive tabulation. Combust Theor Model 1997;1:41–63.
[14] Lu L, Pope SB. An improved algorithm for in situ adaptive tabulation. J Comput Phys 2009;228:361–86.
[15] Damour C, Benne M, Lebreton C, Deseure J, Grondin-Perez B. Real-time implementation of a neural model-based self-tuning PID strategy for oxygen stoichiometry control in PEM fuel cell. Int J Hydrogen Energy 2014;39:12819–25.
[16] Hatti M, Tioursi M. Dynamic neural network controller model of PEM fuel cell system. Int J Hydrogen Energy 2009;34:5015–21.
[17] Szabłowski Ł, Milewski J, Badyda K, Kupecki J. ANN–supported control strategy for a solid oxide fuel cell working on demand for a public utility building. Int J Hydrogen Energy 2018;43:3555–65.
[18] Yap WK, Ho T, Karri V. Exhaust emissions control and engine parameters optimization using artificial neural network virtual sensors for a hydrogen-powered vehicle. Int J Hydrogen Energy 2012;37:8704–15.
[19] Deb M, Majumder P, Majumder A, Roy S, Banerjee R. Application of artificial intelligence (AI) in characterization of the performance–emission profile of a single cylinder CI engine operating with hydrogen in dual fuel mode: an ANN approach with fuzzy-logic based topology optimization. Int J Hydrogen Energy 2016;41:14330–50.
[20] Taghavifar H, Taghavifar H, Mardani A, Mohebbi A, Khalilarya S, Jafarmadar S. On the modeling of convective heat transfer coefficient of hydrogen fueled diesel engine as affected by combustion parameters using a coupled numerical-artificial neural network approach. Int J Hydrogen Energy 2015;40:4370–81.
[21] Syed J, Baig RU, Algarni S, Murthy YVVS, Masood M, Inamurrahman M. Artificial Neural Network modeling of a hydrogen dual fueled diesel engine characteristics: an experiment approach. Int J Hydrogen Energy 2017;42:14750–74.
[22] Zamaniyan A, Joda F, Behroozsarand A, Ebrahimi H. Application of artificial neural networks (ANN) for modeling of industrial hydrogen plant. Int J Hydrogen Energy 2013;38:6289–97.
[23] Kenanoğlu R, Baltacıoğlu MK, Demir MH, Erkınay Özdemir M. Performance & emission analysis of HHO enriched dual-

fuelled diesel engine with artificial neural network prediction approaches. Int J Hydrogen Energy 2020. https://doi.org/10.1016/j.ijhydene.2020.02.108.
[24] An J, Wang H, Liu B, Luo KH, Qin F, He GQ. A deep learning framework for hydrogen-fueled turbulent combustion simulation. Int J Hydrogen Energy 2020;45:17992–8000.
[25] Mordjaoui M, Haddad S, Medoued A, Laouafi A. Electric load forecasting by using dynamic neural network. Int J Hydrogen Energy 2017;42:17655–63.
[26] Seyhan M, Akansu YE, Murat M, Korkmaz Y, Akansu SO. Performance prediction of PEM fuel cell with wavy serpentine flow channel by using artificial neural network. Int J Hydrogen Energy 2017;42:25619–29.
[27] Xue X. Prediction of daily diffuse solar radiation using artificial neural networks. Int J Hydrogen Energy 2017;42:28214–21.
[28] Christo FC, Masri AR, Nebot EM. Artificial neural network implementation of chemistry with pdf simulation of H-2/CO2 flames. Combust Flame 1996;106:406–27.
[29] Blasco JA, Fueyo N, Dopazo C, Ballester J. Modelling the temporal evolution of a reduced combustion chemical system with an artificial neural network. Combust Flame 1998;113:38–52.
[30] Blasco J, Fueyo N, Dopazo C, Chen JY. A self-organizing-map approach to chemistry representation in combustion applications. Combust Theor Model 2000;4:61–76.
[31] Chatzopoulos AK, Rigopoulos S. A chemistry tabulation approach via Rate-Controlled Constrained Equilibrium (RCCE) and Artificial Neural Networks (ANNs), with application to turbulent non-premixed CH4/H-2/N-2 flames. Proc Combust Inst 2013;34:1465–73.
[32] Franke LLC, Chatzopoulos AK, Rigopoulos S. Tabulation of combustion chemistry via artificial neural networks (ANNs): methodology and application to LES-PDF simulation of Sydney flame L. Combust Flame 2017;185:245–60.
[33] Strang G. On the construction and comparison of difference schemes. SIAM J Numer Anal 1968;5:506–17.
[34] Kohonen JH T, Kangas J, Laaksonen J. SOM_PAK: the self-organizing map program package. Technical Report A31. Helsinki University of Technology; 1996.
[35] Rumelhart DE, Hinton GE, Williams RJ. Learning representations by back-propagating errors. Nature 1986;323:533–6.
[36] Cao J, Cui H, Shi H, Jiao L. Big data: a parallel particle swarm optimization-back-propagation neural network algorithm based on MapReduce. PloS One 2016;11:e0157551.
[37] Geethanjali M, Raja Slochanal SM, Bhavani R. PSO trained ANN-based differential protection scheme for power transformers. Neurocomputing 2008;71:904–18.
[38] Kingma D, Ba J. Adam: a method for stochastic optimization. In: International conference on learning representations; 2014.
[39] Liu B, He G-q, Qin F, Cao D, Shi L. Simulation of kerosene fueled RBCC Engine based on skeletal mechanism. In: 21st AIAA international space planes and hypersonics technologies conference. Xiamen, China; 2017.
[40] Chaos M, Kazakov A, Zhao Z, Dryer FL. A high-temperature chemical kinetic model for primary reference fuels. Int J Chem Kinet 2007;39:399–414.
[41] Huang Z, He G, Qin F, Wei X. Large eddy simulation of flame structure and combustion mode in a hydrogen fueled supersonic combustor. Int J Hydrogen Energy 2015;40:9815–24.
[42] Huang Z-W, He G-Q, Wang S, Qin F, Wei X-G, Shi L. Simulations of combustion oscillation and flame dynamics in a strut-based supersonic combustor. Int J Hydrogen Energy 2017;42:8278–87.
[43] Huang Z-W, He G-Q, Qin F, Xue R, Wei X-G, Shi L. Combustion oscillation study in a kerosene fueled rocket-based combined-cycle engine combustor. Acta Astronaut 2016;129:260–70.